INCREASING THE AMPACITY OF UNDERGROUND POWER CABLES BY AN APPLICATION OF PHOTOVOLTAIC PAVEMENTS

Conference Paper · October 2018

CITATION
1

READS
132

4 authors, including:

Dardan Klimenta
University of Priština in Kosovska Mitrovica
63 PUBLICATIONS **428** CITATIONS
SEE PROFILE

Miroljub Jevtic
University of Pristina
66 PUBLICATIONS **434** CITATIONS
SEE PROFILE

Bojan Perovic
University of Pristina
36 PUBLICATIONS **140** CITATIONS
SEE PROFILE

POVEĆANJE TRAJNO DOZVOLJENOG OPTEREĆENJA PODZEMNIH ELEKTROENERGETSKIH KABLOVA PRIMENOM FOTONAPONSKIH TROTOARA

INCREASING THE AMPACITY OF UNDERGROUND POWER CABLES BY AN APPLICATION OF PHOTOVOLTAIC PAVEMENTS

Dardan KLIMENTA[1], **Miroljub JEVTIĆ,**
University of Priština in Kosovska Mitrovica, Kosovska Mitrovica, Serbia,

Jelena KLIMENTA,
Independent Consultant in the Field of Urban and Spatial Planning, Niš, Serbia,

Bojan PEROVIĆ,
University of Priština in Kosovska Mitrovica, Kosovska Mitrovica, Serbia

Ovaj članak pokazuje da se značajno povećanje trajno dozvoljenog opterećenja nekog podzemnog kablovskog voda može postići ako se na celoj dužini istog primeni fotonaponski trotoar u kombinaciji s ventilacionim kanalom i ako se kablovski rov kompletno ispuni termički stabilnom posteljicom s ciljem da se poboljša odvođenje toplote od kablovskog voda. Dodatna prednost korišćenja fotonaponskog trotoara je to što proizvodi električnu energiju. Ovaj članak razmatra i ovo pitanje. Studija slučaja koja uključuje 110 kV kablovski vod predstavljena je s ciljem da se pokaže kako brzina vazduha u ventilacionom kanalu i solarna iradijansa utiču na trajno dozvoljeno opterećenje 110 kV kablovskog voda. U razmatranoj studiji slučaja dobijeno je da se trajno dozvoljeno opterećenje može značajno povećati. Ovo je provereno numerički primenom metode konačnih elemenata u COMSOL-u.

Ključne reči: *elektroenergetski kabl; fotonaponski trotoar; metoda konačnih elemenata; trajno dozvoljeno opterećenje; ventilacioni kanal*

This article shows that a significant increase in the ampacity of an underground cable line can be achieved, if a photovoltaic pavement in combination with a ventilation channel is applied along the entire length of the line, and if the cable trench is completely filled with thermally stable bedding in order to improve the conduction of heat away from the cable line. An additional advantage of using the photovoltaic pavement is that it generates electricity. The present article examines this issue as well. A case study involving a 110 kV cable line is presented to show how the velocity of the air in the ventilation channel and solar irradiance affect the ampacity of the 110 kV cable line. In the considered case study, it is found that the ampacity can be significantly increased. This is verified numerically using the finite-element method in COMSOL.

Key words: *ampacity; finite-element method; photovoltaic pavement; power cable; ventilation channel*

1 Introduction

Surface temperatures of a photovoltaic (PV) pavement can be lower by 11-15 °C and 13-18 °C, respectively, compared with surface temperatures of conventional asphalt pavements and surrounding soils [1]. This can be used in power cable engineering to increase the ampacity of underground power cables. In connection with this, the thermal conductivities of the ethylene-vinyl acetate (EVA) layers in PV pavements are usually lower than the thermal conductivities of thermally stable bedding materials [2-5], and PV cells generate heat along with electricity. In particular, these thermal conductivities and heat sources represent barriers to conductive heat transfer between the cables and the earth surface, while the cable bedding represents a conductive path between them. The effect of thermal con-

[1] Corresponding author: dardan.klimenta@pr.ac.rs

ductivities of EVA composite encapsulants can be effectively eliminated by filling the EVA with the thermally conductive fillers [2,3], and the effect of heat generated in the PV cells can be reduced with a ventilation channel or a system for forced cooling. In this paper, the effect of cable bedding size is not considered because it is assumed that the trench is completely filled with bedding, that there is a ventilation channel in the trench and that the surface of the trench is paved with PV floor tiles.

When PV cells are not exposed to sunlight, they do not generate electricity. In that case, a PV pavement behaves as a cool pavement, and the experimental results from [4,5] can be used to analyze the effect of the equivalent thermal conductivity of the PV pavement on the conduction of heat from a cable (or cables) to the earth surface. These experimental data refer to the cool pavements, and were obtained by laboratory simulations using a physical model of an underground cable. This means that during the execution of the experiments, there was no effect of solar radiation on the experimental apparatus. According to [1] the thermal emissivity of the PV pavement surface is 0.89 and is comparable to the thermal emissivities of the cool pavements from [4,5], which amounted to between 0.9 and 0.94. In this manner, it is ensured that there is an experimental background required for performing simulations using small- and large-size FEM-based models in COMSOL. The small-size model corresponds to the experimental apparatus from [4,5], while the large-size model corresponds to a case study of a 110 kV underground cable line in combination with the PV pavement and ventilation channel.

The thermal effects of the solar absorptivity of the PV pavement surface and convection in the ventilation channel on the ampacity of 110 kV cable line are quantified through the mentioned case study. In this case study, the effect of the most unfavorable ambient conditions during the summer period is considered. The results obtained for the 110 kV cable line installed parallel to the PV pavement and ventilation channel are compared with the corresponding results obtained in [4] for the same line installed parallel to the cool pavements. In addition, on the basis of experimental data for PV pavements from [6,7], four additional operation regimes for the given 110 kV cable line are formulated and considered. Finally, it is established that the ampacity of the 110 kV underground cable line can be significantly increased if the earth surface above the line is covered with PV floor tiles ventilated by forced convection.

2 Experimental background and validation of the method

Since the thermal emissivities of PV pavements are similar to the thermal emissivities of concrete surface, acrylic white paint and acrylic black paint, it is evident that the experimental results reported in [4,5] can be used as an experimental background for the purposes of this paper. This applies only when PV cells are not exposed to sunlight and when the equivalent thermal conductivity of a PV pavement is close or equal to the thermal conductivity of concrete blocks of 1.3 $W \cdot m^{-1} \cdot K^{-1}$ [4,5]. The main function of the experimental apparatus was to simulate the effects of the thermal emissivity ε and solar absorptivity α of the different pavement surfaces on the thermal environment of an underground power cable under known ambient conditions in a laboratory; where the effect of the inner walls of that laboratory was equivalent to the effect of solar irradiance. Some photographs of the experimental apparatus are shown in Figure 1. The photographs illustrate the following: (a) power supply and all used devices, (b) pavement made of concrete blocks, (c) concrete pavement coated with acrylic white paint, and (d) concrete pavement coated with acrylic black paint.

In the experiments, an uninsulated copper pipe reproduced the cable, a round tubular heater (having a total nominal power of 800 W) reproduced sources of heat in the cable, river sand reproduced the cable bedding, 65-mm-thick concrete blocks reproduced the pavement, and inner surfaces of the container represented the bedding edges. The container was made from a used refrigerator, filled with river sand up to 75 mm below its top edges, and covered with concrete blocks. For all the outer surfaces of the container (except for the upper surface of the pavement), the heat transfer coefficient amounted approximately to 3 $W \cdot m^{-2} \cdot K^{-1}$. The heater was connected to the low-voltage power supply network by means of a temperature regulator and an auxiliary relay. The space between the heater and the inner surface of the copper pipe was filled with mineral motor oil. The J-type thermocouples were installed on the copper pipe in four different locations (one in the air, and three in the sand), including the inner lateral surface of the container, the lower surface of the pavement, the upper surface of the pavement, and the air surrounding the apparatus [4]. The first thermocouple was connected to the

measuring input of temperature regulator, while the other seven thermocouples were connected to a data acquisition system. The data acquisition system was connected to a laptop in order to collect the measured temperatures. Temperatures of the outer lateral surfaces of the container were measured by an infrared thermometer [4]. More details on these experiments can be found in [4,5]. The schematic diagram of the experimental apparatus is also given in the aforementioned papers.

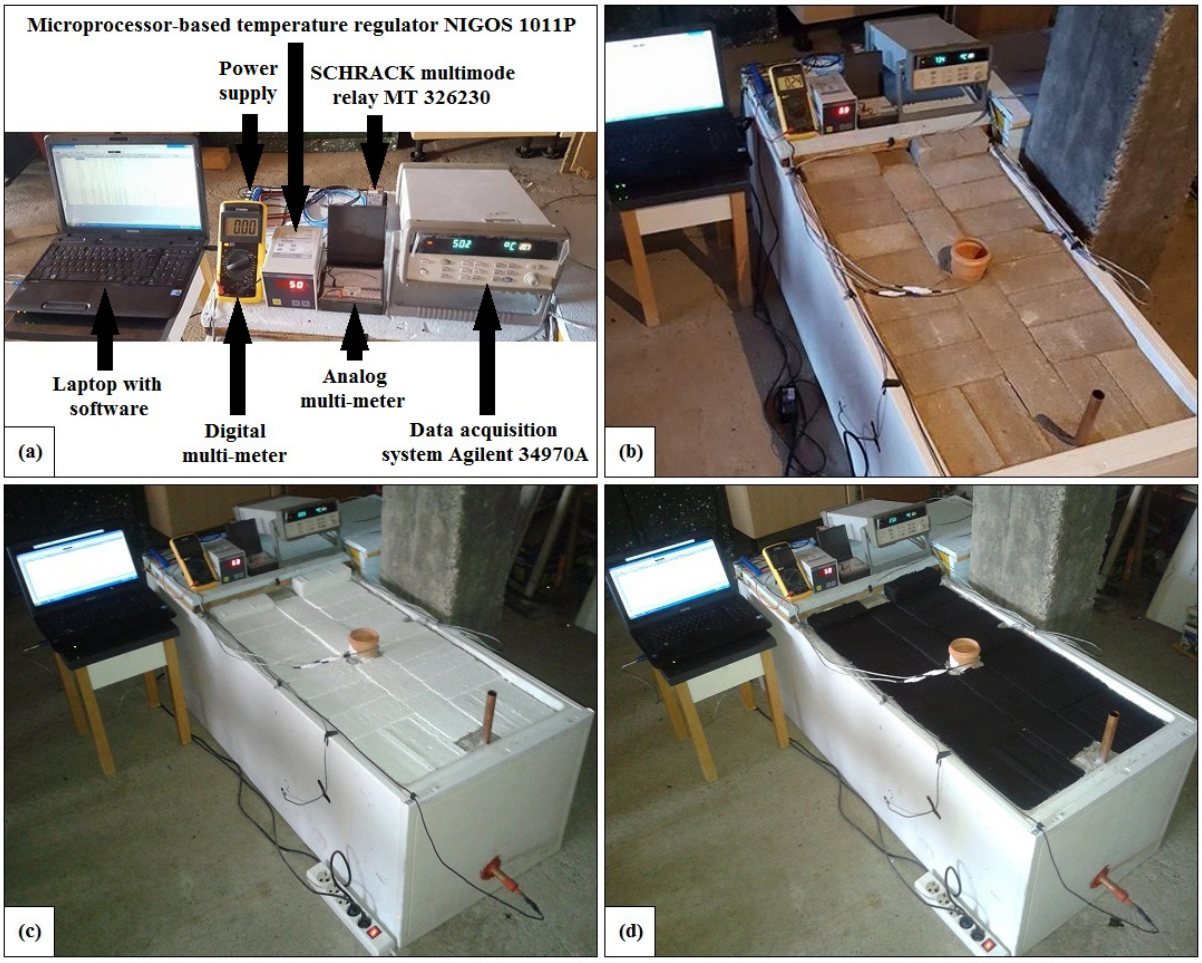

Figure 1. Photographs of the experimental apparatus: (a) power supply and devices, (b) apparatus with a grey surface, (c) apparatus with a white surface, and (d) apparatus with a black surface.

The references [4] and [5] provide more details related to the experimental results, measurement procedure, governing equation, boundary conditions, heat sources and other material properties.

If the pavement from the aforementioned experiments is replaced by a sandwich composed of 21.18-mm-thick PV floor tiles and 43.82-mm-thick concrete blocks, a structure of identical thickness would be obtained. In this case, PV floor tiles would represent the PV pavement, and the concrete blocks would represent its base layer. A computational domain of small-size corresponding to such experimental apparatus and the cross-section of the considered PV floor tile are given in Figures 2a and 2b, respectively. The thermal conductivities of the materials appearing in Figure 2a are given in [4,5], while the equivalent thermal conductivity of the PV floor tile in Figure 2b is 1.02 $W \cdot m^{-1} \cdot K^{-1}$.

The results obtained by simulating the temperature field distribution over the computational domain in Figure 2a are reported in Table 1. This table outlines the simulation results obtained for the actual laboratory conditions from [4,5], i.e. for temperature of the surrounding air T_a=23 °C, wind velocity v_a=0 $m \cdot s^{-1}$, coefficient which takes into account heat transfer due to convection between the PV pavement surface and the surrounding air h=7.382 $W \cdot m^{-2} \cdot K^{-1}$ and solar irradiance $Q_{S,s}$=0 $W \cdot m^{-2}$. According to [6,7], the thermal emissivity and solar absorptivity of the upper surface of the considered PV floor tiles are 0.89 and 0.927, respectively. Based on these values, it is obvious that the simulation

results obtained for the PV floor tiles can be compared with the experimental results obtained in [4,5] for the concrete pavement coated with acrylic black paint. The temperature differences between the simulation results and corresponding experimental values are listed in Table 2.

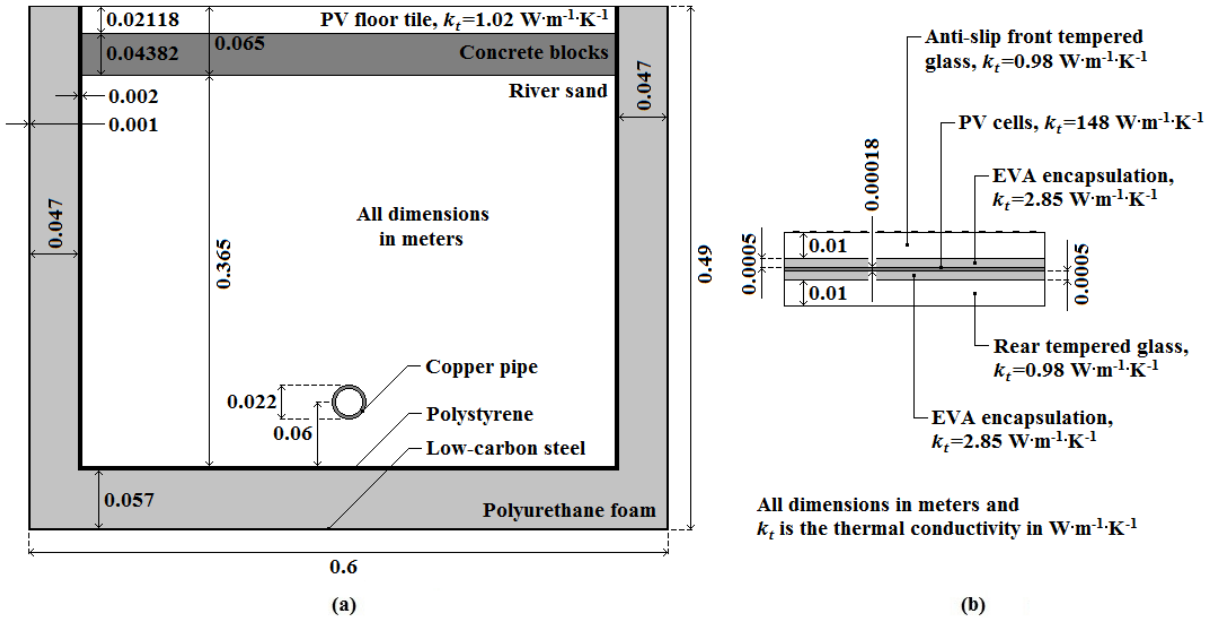

Figure 2. (a) Computational domain of small-size corresponding to the experimental apparatus with PV floor tiles, and (b) PV floor tile configuration.

Table 1. Simulation results obtained using the computational domain in Figure 2a for the actual laboratory conditions.

Experiment	*PV pavement surface*	*Temperature* [°C]		
	Emissivity [–]	*Copper pipe*	*Lower surface of concrete blocks*	*Upper surface of PV floor tiles*
1	0.89	60	26.02	24.77
2	0.89	65	26.42	25.01
3	0.89	70	26.83	25.25

Table 2. Temperature differences between the values calculated for the domain in Figure 2a and the experimental values obtained for the concrete pavement coated with acrylic black paint.

Experiment	*PV pavement surface*	*Temperature difference* [°C] *		
	Emissivity [–]	*Copper pipe*	*Lower surface of concrete blocks*	*Upper surface of PV floor tiles*
1	0.89	-1.0	-0.78	-1.13
2	0.89	-0.8	-0.88	-1.29
3	0.89	-0.7	-0.27	-0.65

* Temperature differences are calculated for the actual laboratory conditions.

When the simulation results from Table 1 are compared with the corresponding experimental data in [4,5], the following observations can be made: (i) For each temperature of the copper pipe, under known laboratory conditions, approximately the same temperature distribution is obtained regardless of the type of the pavement surface. (ii) The calculated temperature of the copper pipe is lower by 0.7-1.0 °C than the corresponding average temperature of the copper pipe obtained for the black

concrete-pavement surface. (iii) The difference between the calculated temperature of the lower surface of the concrete layer below the PV floor tiles and its corresponding value measured for the black concrete-pavement surface ranges from -0.27 °C to -0.88 °C. (iv) The difference between the calculated temperature of the upper surface of the PV floor tiles and its corresponding value measured for the black concrete-pavement surface ranges from -0.65 °C to -1.29 °C. The first observation is based on approximately equal values for the emissivity of the considered surfaces, while the remaining three observations indicate a satisfactory level of accuracy on account of the created model.

The thermal effect of the laboratory interior on the upper surface of the PV floor tiles in the experimental apparatus would be equivalent to the thermal effect of outdoor solar radiation. For the upper surface of the PV pavement the product $\alpha \cdot Q_{S,s}$ equals 388.17 W·m^{-2}. This means that the results from Table 1 would also be obtained in the case that the experimental apparatus was located outdoors and that the solar irradiance $Q_{S,s}$ corresponding to the previously given product $\alpha \cdot Q_{S,s}$ was incident on the pavement surface. If $Q_{S,s}$ was 0 W·m^{-2}, significantly lower temperatures would correspond to each particular case from Table 1. More details related to this issue can be found in [4,5].

3 Computational domain of large-size

Computational domain of large-size which will be used for confirmation of the initial assumption that the ampacity of underground power cables can be increased by the PV pavement is shown in Figure 3a. The considered cables are of the type AXLJ 1×1000/190 mm^2 110 kV, and the dimensions of their structural elements are given in Figure 3b. Abbreviations appearing in Figure 3 have the following meanings: XLPE – cross-linked polyethylene, PE – polyethylene and HDPE – high-density polyethylene.

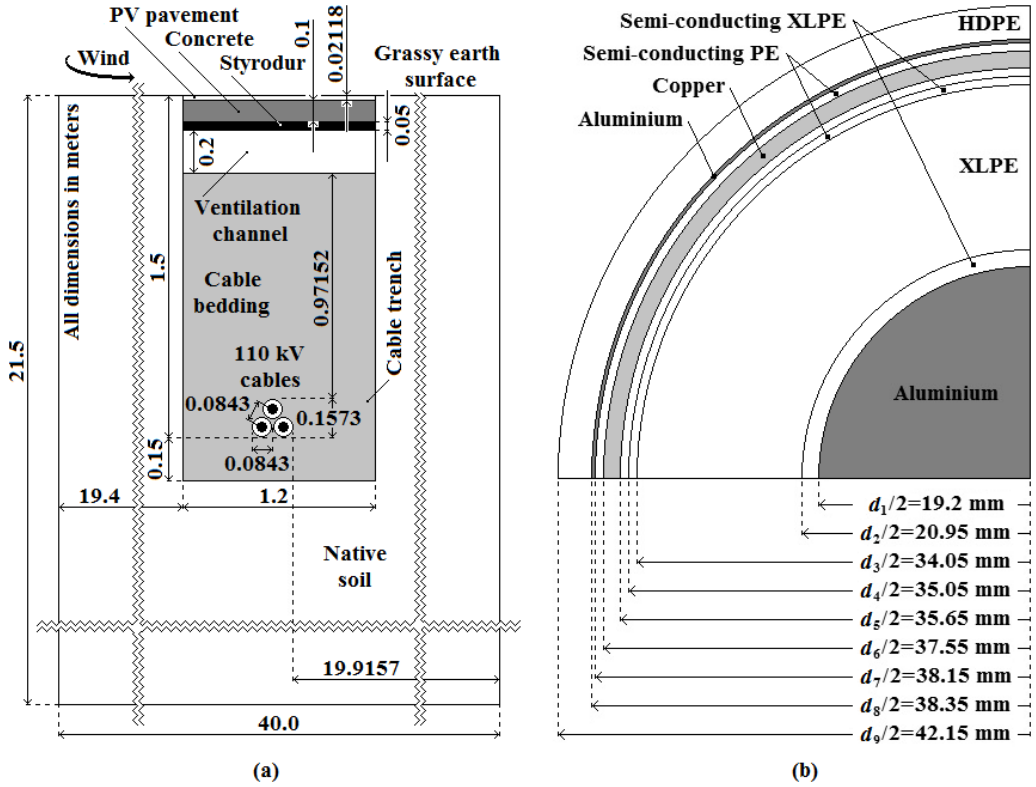

Figure 3. (a) Computational domain of large-size, and (b) dimensions of the construction elements of the AXLJ 1×1000/190 mm^2 110 kV cable.

Figure 3a shows the computational domain for the case when the cable trench is completely filled with the bedding material. Compared with the computational domain in Figure 2a, the dimensions of the domain in Figure 3a are large and selected in accordance with the rule saying that external boundaries of a computational domain should be positioned in places where the constant temperature and homogenous boundary conditions are satisfied simultaneously [8].

For the purposes of simulations using the COMSOL Multiphysics software, the AXLJ 1×1000/190 mm^2 110 kV cables are modeled by an equivalent construction composed of the aluminium conductor, XLPE insulation, copper screen and outer PE sheath with outer diameters d_1, d_5, d_8 and d_9, respectively. According to [8], the equivalent construction is created in the following manner: (i) the semi-conducting screens and swelling tapes under the metal screen are added to the block representing the XLPE insulation; and (ii) the swelling tapes over the metal screen and water-sealing aluminium layer are modeled by an equivalent metal screen with thermal properties of copper. The outer diameters d_1-d_9 are indicated in Figure 3b.

4 Steady-state operation regimes

FEM simulations of steady-state temperature distribution over the domain in Figure 3a are conducted for the following eight cases of operation regimes:

1. Temperature of the air contacting the earth surface T_a=40 °C, wind velocity v_a=0.22 m·s^{-1}, solar irradiance $Q_{S,s}$=1000 W·m^{-2}, power output of one PV floor tile Q_{el}=19.92 W, equivalent volume power of heat sources in the PV floor tiles Q_{PV}=40005.7 W·m^{-3}, heat transfer coefficient due to convection between the PV floor tiles and the air h_{PV}=8 W·m^{-2}·K^{-1}, heat transfer coefficient due to convection between the grassy earth surface and the air h_{GES}=12.654 W·m^{-2}·K^{-1}, velocity of the air in the ventilation channel (i.e. interior air) v_{ai}=0 m·s^{-1}, heat transfer coefficient due to convection between the upper surface of the ventilation channel and the interior air h_{cu}=1.82 W·m^{-2}·K^{-1}, heat transfer coefficient due to convection between the bottom surface of the ventilation channel and the interior air h_{cb}=4.795 W·m^{-2}·K^{-1}, and heat transfer coefficient due to convection between the lateral surfaces of the ventilation channel and the interior air h_{cl}=4.074 W·m^{-2}·K^{-1}.
2. T_a=40 °C, v_a=0.22 m·s^{-1}, $Q_{S,s}$=1000 W·m^{-2}, Q_{el}=19.92 W, Q_{PV}=40005.7 W·m^{-3}, h_{PV}=8 W·m^{-2}·K^{-1}, h_{GES}=12.654 W·m^{-2}·K^{-1}, v_{ai}=0.5 m·s^{-1}, h_{cu}=2.159 W·m^{-2}·K^{-1}, h_{cb}=6.413 W·m^{-2}·K^{-1}, and h_{cl}=5.459 W·m^{-2}·K^{-1}.
3. T_a=40 °C, v_a=0.22 m·s^{-1}, $Q_{S,s}$=1000 W·m^{-2}, Q_{el}=19.92 W, Q_{PV}=40005.7 W·m^{-3}, h_{PV}=8 W·m^{-2}·K^{-1}, h_{GES}=12.654 W·m^{-2}·K^{-1}, v_{ai}=1 m·s^{-1}, h_{cu}=2.543 W·m^{-2}·K^{-1}, h_{cb}=7.55 W·m^{-2}·K^{-1}, and h_{cl}=7.233 W·m^{-2}·K^{-1}.
4. T_a=40 °C, v_a=0.22 m·s^{-1}, $Q_{S,s}$=1000 W·m^{-2}, Q_{el}=19.92 W, Q_{PV}=40005.7 W·m^{-3}, h_{PV}=8 W·m^{-2}·K^{-1}, h_{GES}=12.654 W·m^{-2}·K^{-1}, v_{ai}=2 m·s^{-1}, h_{cu}=3.312 W·m^{-2}·K^{-1}, h_{cb}=9.392 W·m^{-2}·K^{-1}, and h_{cl}=10.915 W·m^{-2}·K^{-1}.
5. T_a=25 °C, v_a=0 m·s^{-1}, $Q_{S,s}$=1000 W·m^{-2}, Q_{el}=21.2 W, Q_{PV}=39764.4 W·m^{-3}, h_{PV}=6.782 W·m^{-2}·K^{-1}, h_{GES}=11.4 W·m^{-2}·K^{-1}, v_{ai}=1 m·s^{-1}, h_{cu}=2.543 W·m^{-2}·K^{-1}, h_{cb}=7.55 W·m^{-2}·K^{-1}, and h_{cl}=7.233 W·m^{-2}·K^{-1}.
6. T_a=25 °C, v_a=0 m·s^{-1}, $Q_{S,s}$=960 W·m^{-2}, Q_{el}=20.5 W, Q_{PV}=38149.2 W·m^{-3}, h_{PV}=6.782 W·m^{-2}·K^{-1}, h_{GES}=11.4 W·m^{-2}·K^{-1}, v_{ai}=1 m·s^{-1}, h_{cu}=2.543 W·m^{-2}·K^{-1}, h_{cb}=7.55 W·m^{-2}·K^{-1}, and h_{cl}=7.233 W·m^{-2}·K^{-1}.
7. T_a=25 °C, v_a=0 m·s^{-1}, $Q_{S,s}$=863 W·m^{-2}, Q_{el}=18.6 W, Q_{PV}=34258.7 W·m^{-3}, h_{PV}=6.782 W·m^{-2}·K^{-1}, h_{GES}=11.4 W·m^{-2}·K^{-1}, v_{ai}=1 m·s^{-1}, h_{cu}=2.543 W·m^{-2}·K^{-1}, h_{cb}=7.55 W·m^{-2}·K^{-1}, and h_{cl}=7.233 W·m^{-2}·K^{-1}.
8. T_a=25 °C, v_a=0 m·s^{-1}, $Q_{S,s}$=615 W·m^{-2}, Q_{el}=13.7 W, Q_{PV}=24324.8 W·m^{-3}, h_{PV}=6.782 W·m^{-2}·K^{-1}, h_{GES}=11.4 W·m^{-2}·K^{-1}, v_{ai}=1 m·s^{-1}, h_{cu}=2.543 W·m^{-2}·K^{-1}, h_{cb}=7.55 W·m^{-2}·K^{-1}, and h_{cl}=7.233 W·m^{-2}·K^{-1}.

The remaining parameters which are the same for all of these operation regimes are as follows: equivalent thermal conductivity of the PV floor tiles k_{PV}=0.8555 W·m^{-1}·K^{-1}, continuously permissible temperature of the considered XLPE cables T_{cp}=90 °C, thermal emissivity of the upper surface of the PV floor tiles ε_{PV}=0.89, thermal emissivity of the grassy earth surface ε_{GES}=0.94, solar absorptivity of

the upper surface of the PV floor tiles α_{PV}=0.927, solar absorptivity of the grassy earth surface α_{GES}=0.6, thermal conductivity of the cable bedding in a dried-out state k_{cb}=1 W·K^{-1}·m^{-1}, thermal conductivity of the native soil in a dried-out state k_{ns}=0.4 W·K^{-1}·m^{-1}, thermal conductivity of concrete k_c=1.3 W·m^{-1}·K^{-1}, thermal conductivity of styrodur k_{ti}=0.033 W·m^{-1}·K^{-1}, thermal conductivity of aluminium k_{Al}=239 W·m^{-1}·K^{-1}, thermal conductivity of XLPE k_{XLPE}=0.286 W·m^{-1}·K^{-1}, thermal conductivity of copper k_{Cu}=385 W·m^{-1}·K^{-1}, and thermal conductivity of PE k_{PE}=0.286 W·m^{-1}·K^{-1}.

The values of the coefficients h_{cu}, h_{cb} and h_{cl} are estimated using empirical correlations from [9] for the case that the difference between the temperature of the channel walls and the temperature of the interior air is 10 °C. The first four operation regimes are chosen so that the obtained results are comparable to the results obtained for traditional and cool pavements in [4], while the remaining four are chosen to demonstrate how the solar irradiance affects the conduction of heat from cables to the earth surface. It is also assumed that the thickness of the structure composed of PV floor tiles, concrete and styrodur (thermal insulation) equals 0.17118 m for each of the eight cases and that there are grassy areas on the both sides of the PV pavement.

5 Results and discussion

In order to generalize the results obtained for the small-size domain, the large-size FEM-based model with 110 kV cables was created and represented geometrically in Figure 3a. For the purposes of determining the ampacity of the 110 kV cable line I_{cp}, two sequences of simulations over this computational domain are performed. The first sequence of simulations is performed with the solar irradiance of 1000 W·m^{-2} and the following four velocities of the air in the ventilation channel: 0, 0.5, 1 and 2 m·s^{-1} (operation regimes 1-4). The second sequence of simulations is performed with the velocity of the air in the ventilation channel of 1 m·s^{-1} and the following four values of the solar irradiance: 1000, 960, 863 and 615 W·m^{-2} (operation regimes 5-8). The values for the volume power of heat sources Q_v are gradually increased from an arbitrary prescribed initial value (for instance 1.5 kW·m^{-3}) to its continuously permissible value (corresponding to the temperature T_{cp}=90 °C). Then, these volume powers of heat sources and the corresponding equation from [4] are used to calculate the cable ampacities. The results corresponding to the first and second sequences of simulations are given in Tables 3 and 4, respectively.

Table 3. Volume powers of heat sources in cables' conductors Q_v and ampacities I_{cp} calculated for a constant solar irradiance $Q_{S,s}$=1000 W·m^{-2} and different velocities of the interior air v_{ai}.

Thermal environment	α/ε [–]	v_{ai} [m·s^{-1}]	Q_v [W·m^{-3}]	I_{cp} [A]
Figure 3a + operation conditions 1	1.042	0.0	15045	652.608
Figure 3a + operation conditions 2	1.042	0.5	15285	657.793
Figure 3a + operation conditions 3	1.042	1.0	15405	660.370
Figure 3a + operation conditions 4	1.042	2.0	15545	663.364

Table 4. Volume powers of heat sources in cables' conductors Q_v and ampacities I_{cp} calculated for different solar irradiances $Q_{S,s}$ and a constant velocity of the interior air v_{ai}=1 m·s^{-1}.

Thermal environment	α/ε [–]	$Q_{S,s}$ [W·m^{-2}]	Q_v [W·m^{-3}]	I_{cp} [A]
Figure 3a + operation conditions 5	1.042	1000	19425	741.544
Figure 3a + operation conditions 6	1.042	960	19620	745.257
Figure 3a + operation conditions 7	1.042	863	20085	754.037
Figure 3a + operation conditions 8	1.042	615	21310	776.691

For the large-size domain, base values for Q_v and I_{cp} are selected in such a manner so that they correspond to surface radiation properties of the traditional asphalt-pavement (α and ε) from [4], thermal conductivity of the asphalt k_{as}=1.2 W·K^{-1}·m^{-1} and continuously permissible temperature of the

cables T_{cp}=90 °C, as follows: Q_v=11260 W·m^{-3} and I_{cp}=564.58 A. All required input parameters are constant and specified in [4].

Concerning the quantification of the effect of the PV pavement in combination with the ventilation channel on the ampacity of the considered 110 kV cable line, the following can be observed: (i) In comparison with the base case (traditional asphalt-pavement), the PV pavement in combination with the ventilation channel can increase the ampacity of the considered 110 kV cable line by 95.79 A when v_{ai}=1 m·s^{-1} and $Q_{S,s}$=1000 W·m^{-2}. (ii) The decrease in the temperature of the air contacting the earth surface from 40 to 25 °C can additionally increase the cable ampacity by 81.174 A when v_{ai}=1 m·s^{-1} and $Q_{S,s}$=1000 W·m^{-2}. (iii) The increase in the velocity of the interior air from 0 to 2 m·s^{-1} can increase the cable ampacity by only 10.756 A when $Q_{S,s}$=1000 W·m^{-2}. (iv) The decrease in the solar irradiance from 1000 to 615 W·m^{-2} can increase the cable ampacity by 35.147 A when v_{ai}=1 m·s^{-1}. This means that the cable ampacity can be significantly increased if the traditional asphalt-pavement is replaced by the PV pavement in combination with the ventilation channel and if the cable trench is completely filled with the bedding material.

In addition to these observations, it is interesting to demonstrate whether the PV pavement can lead to an increase in the cable ampacity if there is no ventilation channel in Figure 3a. The best way to do this is to compare the temperature distribution corresponding to such a computational domain with the temperature distribution corresponding to the base case taken from [4]. In order for these computational domains to be comparable, it is assumed that the total thickness of the PV pavement and the concrete layer below it is 0.05 m and that the same operation conditions apply as in the case of the base case. The isotherms of 50, 60 and 70 °C which are obtained by simulation of the steady-state temperature distribution over these two domains are presented in Figures 4 and 5. Figure 4 shows the isotherms generated within the domain corresponding to the base case, while Figure 5 shows the isotherms generated within the domain with PV pavement and no ventilation channel.

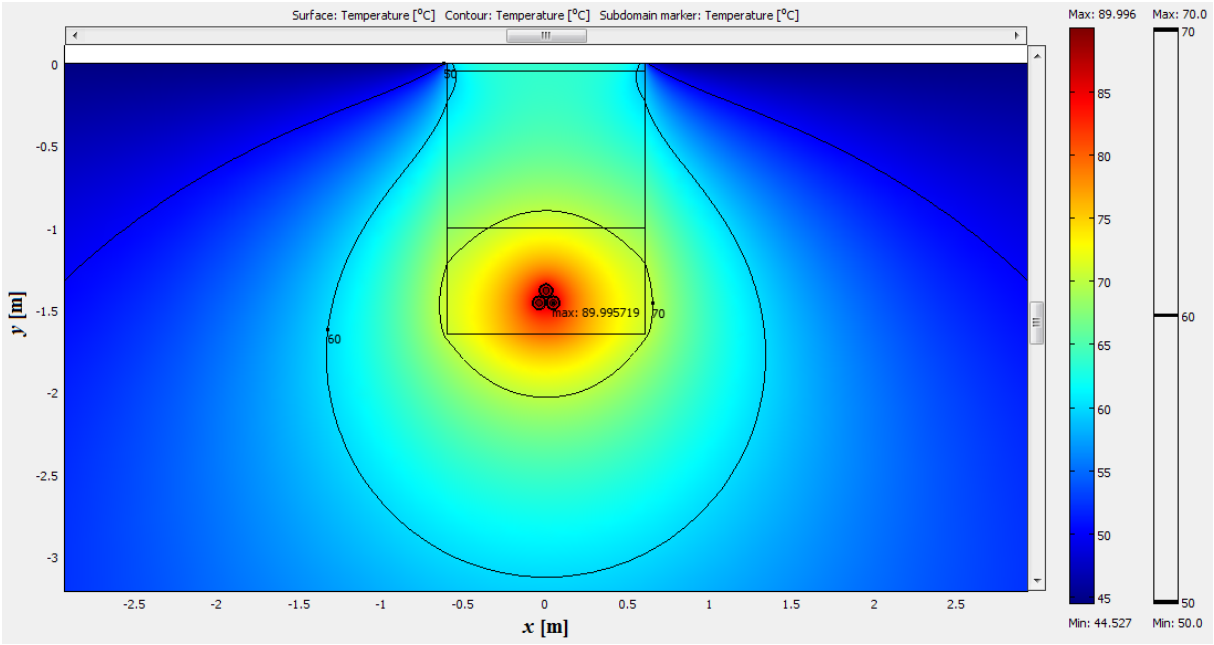

Figure 4. Temperature distribution over the computational domain corresponding to the base case.

Based on the results shown in Figures 4 and 5, for the same cable ampacities, it is more than evident that the temperature of the cables' conductors cannot be decreased below the continuously permissible temperature T_{cp}=90 °C using only the PV pavement (without a ventilation channel). According to these two figures, the maximum conductor temperature of cables in Figure 5 is higher by 4.63 °C than the temperature T_{cp}. When this maximum temperature is equal to 90 °C, the cable ampacity corresponding to the case with the PV pavement is lower by 36.263 A than the cable ampacity corresponding to the base case (i.e. than I_{cp}=564.58 A).

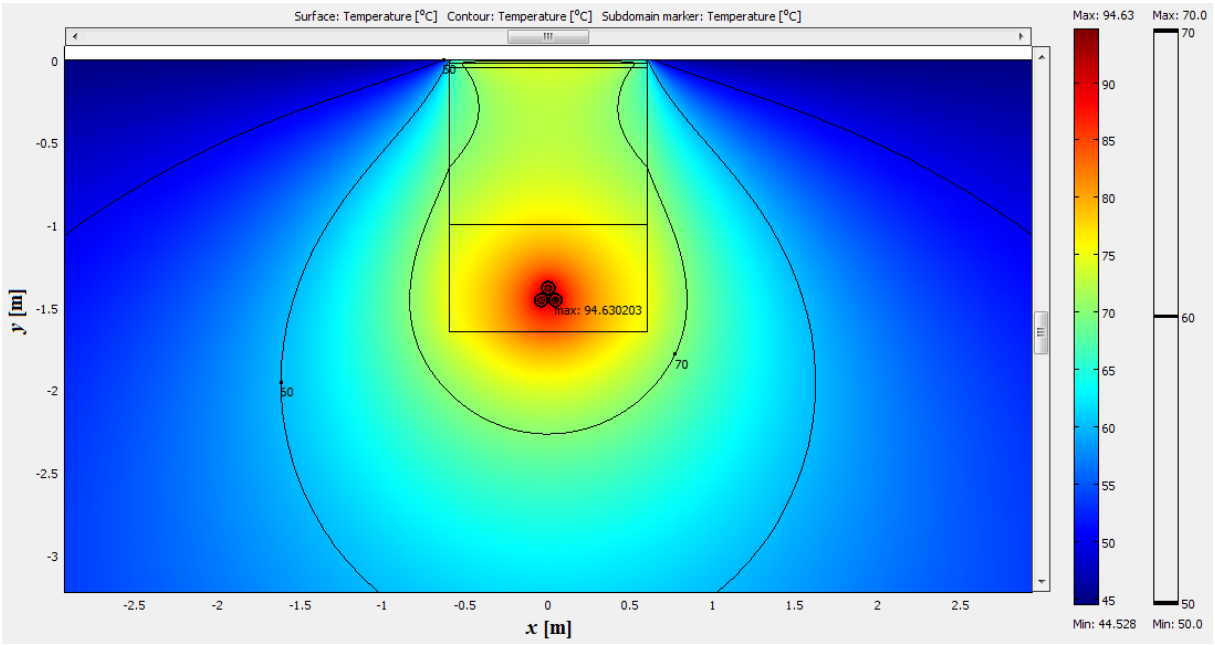

Figure 5. Temperature distribution over the computational domain with PV pavement and no ventilation channel, which is equivalent to the one corresponding to the base case.

6 Conclusions

The main conclusions that can be drawn from the presented results and discussion are:

- Using the PV pavement and ventilation channel, compared to the base case, the ampacity of the considered 110 kV underground cable line can be increased by 98.784 A when the velocity of the air in the ventilation channel is 2 $m \cdot s^{-1}$ and when the solar irradiance is 1000 $W \cdot m^{-2}$.
- Using only the PV pavement without a ventilation channel, the ampacity of the considered 110 kV underground cable line cannot be increased above the ampacity value corresponding to the base case.
- The proposed method for increasing the ampacity of underground cable lines is new, it can be easily implemented within current practice, it would generate enough electricity to meet demand for ventilation and cooling purposes, and it would result in significant economic benefits.
- The increase in the velocity of the interior air from 0 to 2 $m \cdot s^{-1}$ does not significantly affect the ampacity of the considered 110 kV cable line, so that the electricity generated by the PV pavement does not have to be used for forced-air ventilation.

7 Acknowledgement

This paper was based on research conducted within the project TR33046.

8 References

[1] **Efthymiou, C., M. Santamouris, D. Kolokotsa, A. Koras**, Development and testing of photovoltaic pavement for heat island mitigation, *Solar Energy, 130* (2016), pp. 148–160.
[2] **Lee, B., J. Z. Liu, B. Sun, C. Y. Shen, G. C. Dai**, Thermally conductive and electrically insulating EVA composite encapsulants for solar photovoltaic (PV) cell, *eXPRESS Polymer Letters, 2* (2008), 5, pp. 357–363.
[3] **Allan, J., H. Pinder, Z. Dehouche**, Enhancing the thermal conductivity of ethylene-vinyl acetate (EVA) in a photovoltaic thermal collector, *AIP Advances, 6* (2016), 035011, pp. 1–9.
[4] **Klimenta, D., B. Perović, J. Klimenta, M. Jevtić, M. Milovanović, I. Krstić**, Controlling the thermal environment of underground cable lines using the pavement surface radiation properties,

IET Generation, Transmission & Distribution, Available online: April 5, 2018, DOI: 10.1049/iet-gtd.2017.1298.
[5] **Klimenta, D. O., B. D. Perović, J. Lj. Klimenta, M. M. Jevtić, M. J. Milovanović, I. D. Krstić**, Controlling the thermal environment of underground power cables adjacent to heating pipeline using the pavement surface radiation properties, *Thermal Science,* Available online: January 7, 2018, DOI: 10.2298/TSCI171103312K.
[6] **Tao, M., Y. Hongxing, L. Lin**, Development of solar photovoltaic pavement panels for application on the green deck, *World Sustainable Built Environment Conference 2017 Hong Kong (WSBE17 Hong Kong)*, Construction Industry Council (CIC) and Hong Kong Green Building Council (HKGBC), Hong Kong SAR, June 5-7, 2017.
[7] **Hongxing, Y., M. Tao**, *Research and development of solar PV pavement panels for application on the green deck*, Final Report, The Hong Kong Polytechnic University, Hong Kong SAR, 2016.
[8] **Klimenta, D., B. Perovic, M. Jevtic, J. Radosavljevic, N. Arsic**, A thermal FEM-based procedure for the design of energy-efficient underground cable lines, *Humanities and Science University Journal - Technics*, *10* (2014), pp. 162-188.
[9] **Awbi, H. B., A. Hatton**, Mixed convection from heated room surfaces, *Energy and Buildings, 32* (2000), pp. 153–166.